Low-Order Numerical Analysis of Winglet Geometry Effects on the Aerodynamic Characteristics of B737NG and A320 Wings Using Python

Achmad Ferdinand Syach*[1], Ahmad Atif Fikri[2]
[1](Department of Educational Technology, Universitas Negeri Malang, Malang, Indonesia, achmadferdinandsyach@gmail.com)
[2](Department of Educational Technology, Universitas Negeri Malang, Malang, Indonesia, achmadferdinandsyach@gmail.com)
*corresponding author

Received: 2026-June-15
Rev. Req: 2026-June-17
Accepted: 2026-June-20

ABSTRACT: *Winglets are wingtip aerodynamic devices used to mitigate lift-induced drag by weakening wingtip vortices and improving the effective spanwise lift distribution of finite wings. This study develops a reproducible low-order Python framework to compare the aerodynamic characteristics of a B737NG wing representation equipped with a split scimitar winglet and an A320 wing representation equipped with a sharklet. The model combines finite-wing lift-slope correction, induced-drag formulation, a simplified total-drag model, force estimation from dynamic pressure, second-order polynomial regression, and parameter sensitivity analysis. Three angles of attack, namely 0 deg, 5 deg, and 10 deg, were evaluated under pre-stall assumptions. The calculated outputs included lift coefficient, induced drag coefficient, total drag coefficient, lift force, drag force, induced-drag-based lift-to-drag ratio, and total lift-to-drag ratio. The main simulation showed that the highest total lift-to-drag ratio occurred at 5 deg, reaching 17.7567 for the split scimitar winglet and 17.5217 for the sharklet. Polynomial regression estimated local maxima at 6.83 deg and 6.79 deg, respectively. Sensitivity analysis confirmed that increasing the Oswald efficiency factor and effective aspect ratio reduced total drag and increased aerodynamic efficiency. The novelty of this study lies in a transparent Python-only screening workflow that operationalises finite-wing theory for early-stage winglet comparison before higher-fidelity computational fluid dynamics or wind-tunnel validation.*
Keywords: *winglet, induced drag, lift-to-drag ratio, Pyhton, aerodynamic*

ABSTRAK: Winglet adalah perangkat aerodinamis pada ujung sayap yang digunakan untuk mengurangi hambatan akibat gaya angkat (lift-induced drag) dengan melemahkan vorteks ujung sayap dan memperbaiki distribusi gaya angkat efektif sepanjang bentang sayap. Studi ini mengembangkan kerangka kerja Python berorde rendah yang dapat direproduksi untuk membandingkan karakteristik aerodinamis representasi sayap B737NG yang dilengkapi split scimitar winglet dan representasi sayap A320 yang dilengkapi sharklet. Model ini menggabungkan koreksi kemiringan kurva gaya angkat (lift-slope) untuk sayap berhingga, formulasi hambatan induksi, model hambatan total yang disederhanakan, estimasi gaya berdasarkan tekanan dinamis, regresi polinomial orde kedua, dan analisis sensitivitas parameter. Tiga sudut serang—yaitu 0°, 5°, dan 10°—dievaluasi dengan asumsi kondisi sebelum stall. Hasil perhitungan mencakup koefisien gaya angkat, koefisien hambatan induksi, koefisien hambatan total, gaya angkat, gaya hambatan, rasio gaya angkat terhadap hambatan berbasis hambatan induksi, serta rasio gaya angkat terhadap hambatan total. Simulasi utama menunjukkan bahwa rasio gaya angkat terhadap hambatan total tertinggi terjadi pada sudut 5°, mencapai 17,7567 untuk split scimitar winglet dan 17,5217 untuk sharklet. Regresi polinomial mengestimasi nilai maksimum lokal masing-masing pada sudut 6,83° dan 6,79°. Analisis sensitivitas mengonfirmasi bahwa peningkatan faktor efisiensi Oswald dan rasio aspek efektif dapat mengurangi hambatan total serta meningkatkan efisiensi aerodinamis. Kebaruan studi ini terletak pada alur kerja penyaringan yang transparan dan berbasis Python, yang mengoperasionalkan teori sayap berhingga untuk perbandingan awal winglet sebelum dilakukan analisis computational fluid dynamics (CFD) dengan fidelitas lebih tinggi atau validasi menggunakan terowongan angin.

Kata Kunci: *winglet, hambatan induksi, rasio gaya angkat terhadap hambatan, Python, aerodinamis*

I. INTRODUCTION

The introduction of the paper should explain the nature of the problem, previous work, purpose, and the contribution of the paper. The contents of each section may be provided to understand easily about the paper. Aerodynamic efficiency remains a central issue in aircraft design because fuel consumption, operating cost, range, and emissions are strongly related to the ability of the wing to generate lift with minimum drag. A finite wing inevitably produces a three-dimensional flow field at the tip because the pressure difference between the lower and upper wing surfaces drives air around the wingtip. This lateral motion rolls up into a wingtip vortex, modifies the local downwash distribution, reduces the effective angle of attack, and generates an additional drag component known as lift-induced drag. NASA Glenn Research Center explains that wingtip vortices decrease the effective angle of attack and that the induced drag coefficient depends on lift coefficient, aspect ratio, and an efficiency factor. In the modern drag equation, the induced drag coefficient is commonly expressed as the square of the lift coefficient divided by the product of pi, aspect ratio, and the efficiency factor (NASA Glenn Research Center, 2023a, 2023b). Consequently, wingtip devices are not decorative additions; they are aerodynamic interventions intended to reduce the vortex penalty associated with lift production.

Winglets were introduced as a practical solution to reduce wingtip vortex strength without requiring a very large increase in geometric wingspan. Whitcomb (1976) demonstrated through early high-subsonic investigations that properly designed wing-tip-mounted winglets could improve aerodynamic performance by altering the wingtip flow field. NASA Glenn Research Center (2025b) describes the fundamental purpose of a winglet as reducing the strength of the tip vortex so that the flow over the wing becomes more two-dimensional. For transport aircraft, this mechanism is important because increasing aspect ratio by simply extending the span is often limited by structural weight, bending moment, airport gate constraints, manufacturing feasibility, and certification requirements. Therefore, commercial aircraft have adopted several winglet configurations, including blended winglets, split scimitar winglets, raked tips, and sharklets. Each configuration embodies a different compromise among induced-drag reduction, structural loading, wetted area, interference drag, and operating condition.

The theoretical basis for this study is finite-wing aerodynamics. In two-dimensional airfoil theory, lift slope can be approximated by a near-linear relation in the pre-stall region. However, the lift curve of a finite wing differs from the airfoil curve because the induced flow generated by the trailing vortex system changes the effective angle of attack. Anderson (2017) emphasises that finite-wing correction is required because three-dimensional effects modify both lift and induced drag. This relation provides a suitable conceptual foundation for early-stage screening: when the effective aspect ratio and the Oswald efficiency factor improve, induced drag decreases for a given lift coefficient. In practical design terms, the lift-to-drag ratio, L/D, is an efficiency indicator because it compares useful aerodynamic force with the aerodynamic penalty associated with drag.

NASA Glenn Research Center (2024) defines L/D as the lift divided by drag and describes it as an aerodynamic efficiency factor.

Recent winglet research has increasingly relied on computational fluid dynamics (CFD), parametric design, and optimisation. Guerrero et al. (2018) used CFD to investigate the influence of variable cant angle winglets and showed that aerodynamic performance can improve at different angles of attack when the cant angle is adjusted carefully. Guerrero et al. (2020) extended this idea by examining variable cant angle winglets at different flight phases and Mach numbers, thereby highlighting the fact that winglet performance is linked to operating condition rather than a single universal geometry. Vaezi et al. (2025) provided a more recent full factorial investigation of winglet cant angle effects on aerodynamic and aeroacoustic performance, using CFD and screening to compare the importance of cant angle with pressure, temperature, Mach number, and angle of attack. These studies are valuable because they reveal detailed flow physics and multi-parameter interactions, yet they also require considerable modelling effort, mesh generation, turbulence modelling, solver selection, convergence control, and computational resources.

Medium- and low-order aerodynamic models continue to occupy an important position before high-fidelity simulation. Gao et al. (2023) developed an unsteady vortex lattice modelling approach for multi-lifting surfaces using potential-flow assumptions and efficient data structures, demonstrating the relevance of faster aerodynamic computation in design exploration. Joshi and Thomas (2023) reviewed vortex lattice methods for supersonic aircraft design and showed that lower-order tools remain useful when they are placed within the correct validity domain. In aircraft design practice, early analysis often requires rapid iteration, transparent parameter effects, and clear physical interpretation. A low-order model cannot replace CFD or wind-tunnel testing, but it can support preliminary reasoning, educational demonstration, and numerical screening by making the relationships among lift, induced drag, total drag, and L/D explicit.

The current state of the literature therefore contains two important tendencies. First, the most detailed winglet investigations emphasise CFD-based geometry analysis and optimisation. Second, low- and medium-order methods remain useful when the objective is not local flow-field prediction but conceptual comparison, trend evaluation, and reproducible calculation. The present article is positioned between those tendencies. It does not claim to reproduce the complete flow field around a split scimitar winglet or sharklet. Instead, it formulates the two winglet configurations as effective finite-wing representations through aspect ratio and Oswald efficiency factor. This modelling choice deliberately simplifies geometry so that the influence of the governing aerodynamic parameters can be observed clearly.

Table 1 summarises the relevant state of the art and identifies the specific research gap addressed by this study. The table clarifies that prior work has produced strong knowledge on CFD-based cant angle effects, morphing and variable winglets, vortex-lattice modelling, and general finite-wing theory. However, limited attention has been given to a compact Python-only article framework that directly compares two commercial winglet representations using transparent equations, a small numerical dataset, polynomial screening, and sensitivity analysis in a form suitable for engineering computation learning.

Table 1. State-of-the-art mapping and research gap of the present study

Source	Main Focus	Methodological Position	Key Contribution	Remaining Gap for This Study
Whitcomb (1976)	Wing-tip-mounted winglets at high subsonic speeds	Wind-tunnel-oriented design investigation	Established the aerodynamic rationale for winglets as induced-drag reduction devices	Did not provide a modern Python-based reproducible screening framework
Anderson (2017)	Fundamentals of finite-wing aerodynamics	Analytical and textbook formulation	Provides finite-wing lift, induced drag, and aerodynamic force theory	Requires operationalisation into a reproducible computational workflow
Guerrero et al. (2018)	Variable cant angle winglets	CFD at selected aerodynamic conditions	Demonstrated that cant angle influences total drag reduction	High computational burden and no simple low-order educational implementation
Guerrero et al. (2020)	Winglet cant angle for flight performance improvement	CFD across flight phases and Mach numbers	Showed that winglet performance depends on operating condition	Focused on benchmark configurations rather than simplified commercial-winglet comparison
Gao et al. (2023)	Multi-lifting-surface aerodynamics	Unsteady vortex lattice method	Demonstrated faster potential-flow modelling for lifting systems	More advanced than a minimum-equation Python model for introductory screening
Joshi and Thomas (2023)	Vortex lattice method for aircraft design	Review of lower-order aerodynamic tools	Located VLM within preliminary and conceptual design	Did not construct a direct split scimitar versus sharklet numerical article workflow
Vaezi et al. (2025)	Winglet cant angle effects on aerodynamics and aeroacoustics	CFD with full factorial screening	Integrated cant angle, pressure, temperature, Mach number, and angle of attack	Requires CFD datasets and does not target a compact pedagogical low-order framework
Present study	Split scimitar and sharklet representations	Low-order Python numerical model	Links finite-wing equations, polynomial estimation, and sensitivity analysis in one reproducible workflow	Intended as screening before CFD or wind-tunnel validation, not as a final geometry-resolved result

Based on that mapping, the research gap lies in the lack of a compact, fully reproducible, and explicitly documented Python workflow for comparing split scimitar and sharklet representations using low-order aerodynamic parameters. This gap is methodological and educational rather than purely geometric. The novelty is the integration of finite-wing lift-slope correction, induced-drag calculation, total-drag correction, force estimation, polynomial trend estimation, and sensitivity analysis into a single article-scale framework that can be replicated by students, early-stage researchers, and engineering practitioners before proceeding to CFD.

The objective of this study is therefore operational and measurable. First, the study calculates C_L, C_{D_i}, C_D, L, D, L/D_i, and total L/D for split scimitar winglet and sharklet representations at angles of attack of 0 deg, 5 deg, and 10 deg. Second, the study compares both winglet representations using the same air density, free-stream velocity, zero-lift drag coefficient, and zero-angle lift coefficient assumptions. Third, the study estimates the local angle of attack that maximises total L/D using a second-order polynomial fitted to the three simulated points. Fourth, the study evaluates the sensitivity of C_D and total L/D to the Oswald efficiency factor and effective aspect ratio at 5 deg. Fifth, the study states the model limitations explicitly so that the interpretation remains within the valid domain of low-order pre-stall analysis.

II. METHOD

This study used a quantitative computational design. The object of analysis consisted of two simplified winglet representations: a B737NG wing representation with a split scimitar winglet and an A320 wing representation with a sharklet. The term representation is used deliberately because the model does not reconstruct three-dimensional CAD geometry. Instead, the winglet effect is represented through finite-wing parameters, namely reference area, effective aspect ratio, and Oswald efficiency factor. The numerical analysis was implemented using Python syntax compatible with Python 3.x. The computational workflow can be reproduced with standard scientific libraries, namely NumPy for array calculation, pandas for table handling if tabular export is needed, and Matplotlib for graph generation. No commercial CFD solver, mesh generator, turbulence model, or proprietary aerodynamic database is required.

The analysis domain was limited to the pre-stall region. Three angles of attack were selected: 0 deg, 5 deg, and 10 deg. This choice provides a minimum but interpretable dataset for observing the increase in lift coefficient, the quadratic increase in induced drag, and the non-monotonic behaviour of total L/D. The angle of attack was converted into radians before being used in the lift equation. Air density was set at 1.225 kg/m3 and free-stream velocity at 70 m/s. These values were not intended to reproduce a specific certified flight condition; they were chosen as controlled inputs for a comparative low-order calculation. The same values of air density, velocity, zero-angle lift coefficient, and zero-lift drag coefficient were applied to both configurations so that the comparison remained controlled.

The main simulation consisted of six numerical cases: two winglet representations multiplied by three angles of attack. The calculated parameters were divided into input variables, intermediate variables, and output variables. The independent variables were winglet representation and angle of attack. The intermediate variables were finite-wing lift slope, effective aspect ratio, and Oswald efficiency factor. The dependent outputs were C_L, C_{D_i}, C_D, L, D, L/D_i, and total L/D. The control variables were air density, free-stream velocity, reference area, zero-angle lift coefficient, and zero-lift drag coefficient. Table 2 lists the primary simulation parameters.

Table 2. Primary simulation parameters

Winglet Representation	Aircraft Representation	Reference Area, S (m2)	Effective Aspect Ratio, AR	Oswald Efficiency Factor, e	C_L0	C_D0
Split scimitar winglet	B737NG	124.60	9.45	0.86	0.20	0.020
Sharklet	A320	122.60	9.40	0.84	0.20	0.020

The finite-wing lift slope was calculated by correcting the two-dimensional lift slope through aspect ratio and Oswald efficiency factor. The airfoil lift slope was approximated by $a_0 = 2\pi$ rad^-1, which is a common theoretical reference for a thin airfoil in incompressible pre-stall flow. The corrected finite-wing lift slope was calculated as follows:

$$a = \frac{a_0}{1 + \frac{a_0}{\pi e AR}}$$

where a is the finite-wing lift slope, a_0 is the two-dimensional lift slope, e is the Oswald efficiency factor, and AR is the effective aspect ratio. This equation embeds the physical assumption that a higher effective aspect ratio and a higher efficiency factor reduce the downwash penalty and increase the effective lift-slope response of the finite wing.

The lift coefficient was then calculated as a linear function of angle of attack in the pre-stall region:

$$C_L = C_{L0} + a\alpha$$

where C_L is the lift coefficient, C_{L0} is the lift coefficient at zero angle of attack, a is the corrected lift slope, and α is the angle of attack in radians. The induced drag coefficient was calculated using the classical finite-wing relation:

$$C_{D_i} = \frac{C_L^2}{\pi e AR}$$

This equation is central to the study because it expresses the quadratic dependence of induced drag on lift coefficient and the inverse dependence of induced drag on aspect ratio and Oswald efficiency factor. To avoid presenting an unrealistically ideal induced-drag-only model, the total drag coefficient was calculated by adding a zero-lift drag coefficient:

$$C_D = C_{D0} + C_{D_i}$$

where C_D is the total drag coefficient and C_{D0} is the zero-lift drag coefficient. The dynamic pressure was calculated from air density and free-stream velocity:

$$q = \frac{1}{2}\rho V^2$$

Lift and drag forces were calculated using the standard aerodynamic force relation:

$$L = qSC_L$$
$$D = qSC_D$$

where L is lift force, D is drag force, q is dynamic pressure, S is the reference area, and V is free-stream velocity. Two efficiency ratios were used. The first ratio used only induced drag to isolate the induced-drag contribution. The second ratio used total drag and served as the primary aerodynamic efficiency indicator in this study:

$$\frac{L}{D_i} = \frac{C_L}{C_{D_i}}$$

$$\frac{L}{D} = \frac{C_L}{C_D}$$

A second-order polynomial regression was used to estimate the local trend of total L/D as a function of angle of attack. This regression was not intended to create a universal aerodynamic polar. It was used only as a screening approximation from three discrete points. The polynomial form was:

$$\left(\frac{L}{D}\right)(\alpha) = A\alpha^2 + B\alpha + C$$

The stationary point of the polynomial was obtained from the first derivative:

$$\alpha_{\text{ext}} = -\frac{B}{2A}$$

where A, B, and C are polynomial coefficients and α_{ext} is the estimated local extremum. When $A < 0$, the stationary point is interpreted as a local maximum. Because only three angle-of-attack points were used, the estimated optimum was treated as a preliminary indicator, not as a final design optimum.

The numerical procedure followed the workflow shown in Figure 1. The algorithm started by defining the input parameters for each winglet representation. The second step computed finite-wing lift slope, lift coefficient, induced drag coefficient, and total drag coefficient. The third step computed dynamic pressure, lift force, drag force, induced-drag-based L/D_i, and total L/D. The fourth step fitted a second-order polynomial to the total L/D data and conducted sensitivity analysis. The final step checked whether the numerical trends were consistent with finite-wing theory and interpreted the comparative results.

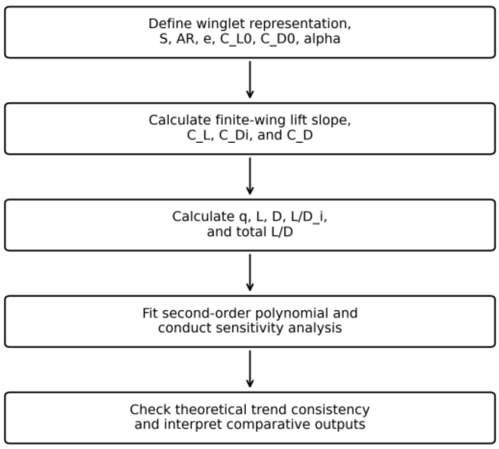

Figure 1. *Workflow of the low-order Python-based numerical simulation.*

The pseudocode used for replication is given in Table 3. The pseudocode is intentionally concise because the model depends on closed-form equations rather than iterative numerical solvers. The replication requirement is therefore satisfied when another researcher can reproduce the input values, equations, loop structure, and output metrics.

Table 3. Reproducible pseudocode of the Python calculation

Step	Pseudocode Operation	Purpose
1	Define constants rho, V, C_L0, C_D0, alpha_deg	Establish controlled simulation conditions

Step	Pseudocode Operation	Purpose
2	Convert alpha_deg to alpha_rad	Ensure dimensional consistency in the lift equation
3	For each winglet representation, define S, AR, and e	Establish comparative input parameters
4	Calculate a = a0 / (1 + a0 / (pi e AR))	Compute finite-wing lift slope
5	Calculate C_L = C_L0 + a alpha	Estimate lift response in the pre-stall range
6	Calculate C_Di = C_L^2 / (pi e AR)	Estimate induced drag from finite-wing theory
7	Calculate C_D = C_D0 + C_Di	Include a simplified non-lifting drag contribution
8	Calculate q, L, D, L/D_i, and L/D	Produce force and efficiency outputs
9	Fit second-order polynomial to L/D versus alpha	Estimate local efficiency maximum
10	Vary e and AR at alpha = 5 deg	Evaluate parameter sensitivity
11	Compare trends with finite-wing theory	Conduct theoretical-trend validation

The validation strategy consisted of theoretical-trend validation and external numerical range comparison. The theoretical-trend validation checked whether the outputs followed the expected structure of the governing equations. The model was considered internally consistent when C_L increased with angle of attack, C_{D_i} increased with C_L^2, C_D increased when C_{D_i} increased, C_D decreased when e or AR increased under controlled conditions, and total L/D improved when induced drag decreased. External numerical validation in the strict CFD or experimental sense was not performed because no geometry-resolved mesh, turbulence model, pressure distribution, or wind-tunnel dataset was generated in this study. Instead, the external comparison was limited to published aerodynamic trends indicating that winglet geometry and operating condition influence drag reduction and L/D (Guerrero et al., 2018, 2020; Vaezi et al., 2025). This distinction is important because it prevents the low-order model from being interpreted as a replacement for CFD.

III. RESULT AND DISCUSSION

Table 4 presents the main numerical results for six simulation cases. The split scimitar winglet representation produced $C_L = 0.2000$, 0.6400, and 1.0800 at 0 deg, 5 deg, and 10 deg, respectively. The sharklet representation produced $C_L = 0.2000$, 0.6375, and 1.0750 for the same angles of attack. The differences are small because both representations used similar reference areas, effective aspect ratios, and Oswald efficiency factors. Nevertheless, the split scimitar representation consistently produced a slightly lower total drag coefficient and a slightly higher total L/D under the assumptions used.

Table 4. Main simulation results for the six numerical cases (SSW = split scimitar winglet; SHK = sharklet)

Rep.	alpha (deg)	C_L	C_Di	C_D	L (N)	D (N)	L/D_i	L/D
SSW	0	0.2000	0.00157	0.02157	74791.15	8064.98	127.6586	9.2736
SSW	5	0.6400	0.01604	0.03604	239340.78	13478.86	39.8918	17.7567
SSW	10	1.0800	0.04569	0.06569	403890.41	24564.58	23.6394	16.4420
SHK	0	0.2000	0.00161	0.02161	73590.65	7952.39	124.0301	9.2539
SHK	5	0.6375	0.01638	0.03638	234568.95	13387.32	38.9116	17.5217
SHK	10	1.0750	0.04659	0.06659	395547.25	24500.50	23.0755	16.1445

Figure 2 shows that C_L increased almost linearly with angle of attack for both representations. This behaviour is expected because the lift model explicitly uses a linear pre-stall relation. The difference between the two curves is caused by the slightly higher AR and e assigned to the split scimitar representation. At 5 deg, the calculated C_L values were 0.6400 and 0.6375 for the split scimitar winglet and sharklet, respectively. Although the numerical difference is only 0.0025, the consistent direction is important because the same difference propagates into induced drag, drag force, and efficiency ratio.

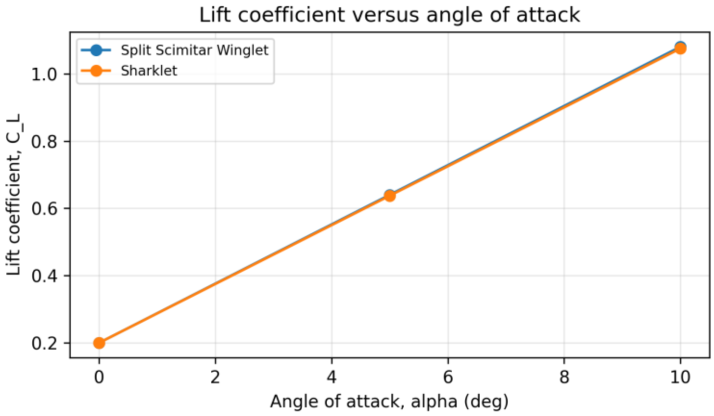

Figure 2. *Lift coefficient versus angle of attack.*

Figure 3 demonstrates the quadratic growth of drag with lift coefficient. Total C_D increased from 0.02157 at 0 deg to 0.06569 at 10 deg for the split scimitar winglet representation. For the sharklet representation, total C_D increased from 0.02161 to 0.06659 over the same range. The sharper increase at 10 deg is consistent with the induced-drag equation because C_{D_i} depends on C_L^2. This result agrees with the aerodynamic principle that increasing angle of attack raises lift but also increases the drag penalty when lift-induced effects become stronger.

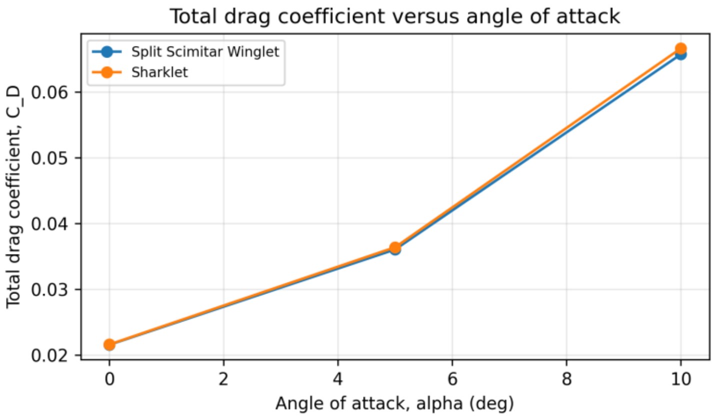

Figure 3. *Total drag coefficient versus angle of attack.*

Figure 4 shows the main aerodynamic efficiency response. Total L/D increased from 0 deg to 5 deg and then decreased at 10 deg for both representations. This non-monotonic behaviour has a clear physical interpretation. At low angle of attack, the increase in lift is large enough to improve L/D even though drag also increases. At higher angle of attack, induced drag grows more rapidly because of its quadratic dependence on C_L, thereby reducing total L/D. The best total L/D in the discrete simulation occurred at 5 deg, with 17.7567 for the split scimitar representation and 17.5217 for the sharklet representation. The split scimitar representation was approximately 1.34% higher than the sharklet at this point, calculated relative to the sharklet value.

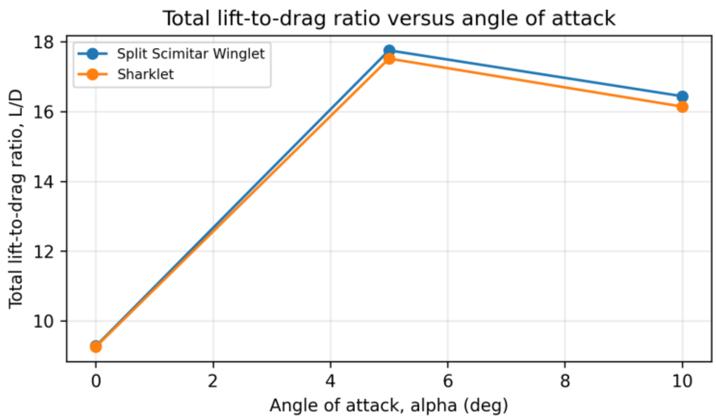

Figure 4. Total lift-to-drag ratio versus angle of attack.

The polynomial regression in Figure 5 was used to estimate the local maximum of total L/D. Table 5 reports that the estimated local maximum occurred at 6.83 deg for the split scimitar winglet and 6.79 deg for the sharklet. The predicted maximum values were 18.4123 and 18.1371, respectively. This result should be interpreted carefully. A polynomial fitted to three points can identify a mathematically smooth trend, but it cannot prove a final aerodynamic optimum. A more robust optimum would require a denser angle-of-attack grid, inclusion of stall behaviour, and comparison with CFD or wind-tunnel data. In the present study, the regression result serves as a screening indicator showing that the best efficiency may occur between 5 deg and 10 deg rather than exactly at one of the simulated points.

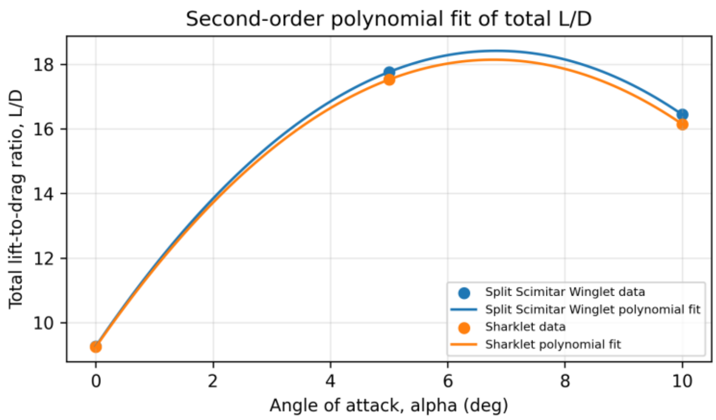

Figure 5. Second-order polynomial fit of total lift-to-drag ratio.

Table 5. Estimated stationary point of the second-order total L/D regression

Winglet Representation	Estimated alpha_ext (deg)	Predicted L/D	Type of Stationary Point
Split scimitar winglet	6.83	18.4123	Local maximum
Sharklet	6.79	18.1371	Local maximum

Figures 6 and 7 compare the induced-drag-only efficiency ratio and total efficiency ratio for each winglet representation. The induced-drag-only L/D_i values were much higher than total L/D values because L/D_i excludes C_{D0}. For example, the split scimitar representation produced $L/D_i = 127.6586$ at 0 deg but total $L/D = 9.2736$ at the same angle. This difference shows why induced-drag-only interpretation can be misleading if it is treated as the total aircraft efficiency. In this article, L/D_i is used only to isolate the contribution of induced drag, whereas total L/D is used as the primary efficiency indicator because it includes both induced drag and simplified zero-lift drag.

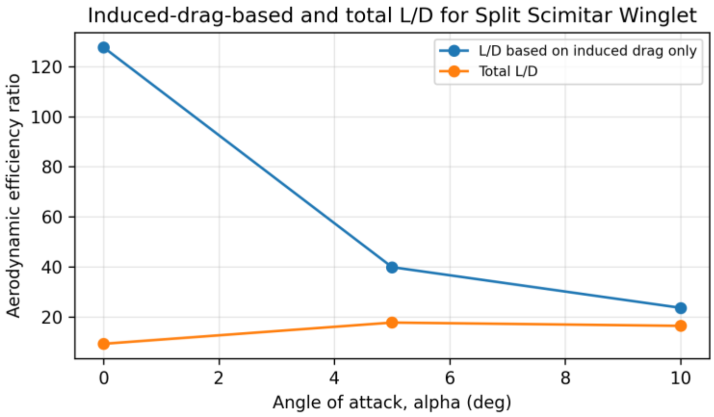

Figure 6. Induced-drag-based and total L/D for the split scimitar winglet representation.

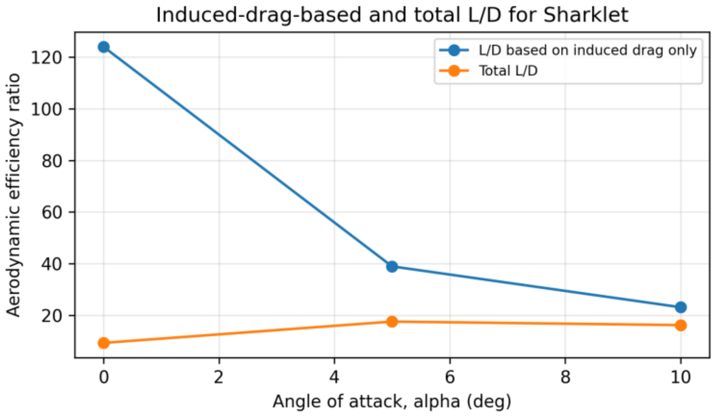

Figure 7. Induced-drag-based and total L/D for the sharklet representation.

The sensitivity analysis in Figures 8 and 9 confirms the role of the Oswald efficiency factor. When e increased from 0.80 to 0.88 at 5 deg, total C_D decreased and total L/D increased for both representations. Physically, a higher e indicates a spanwise lift distribution that is closer to the ideal elliptical distribution. As the lift distribution becomes more efficient, the induced drag component decreases. This trend is directly consistent with the induced-drag equation and supports the internal validity of the model.

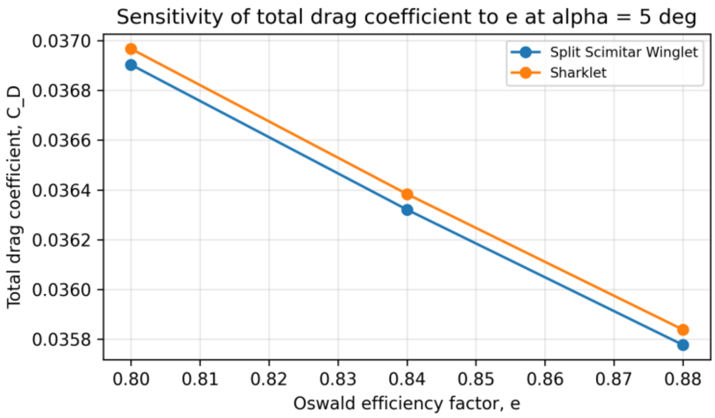

Figure 8. Sensitivity of total drag coefficient to Oswald efficiency factor at alpha = 5 deg.

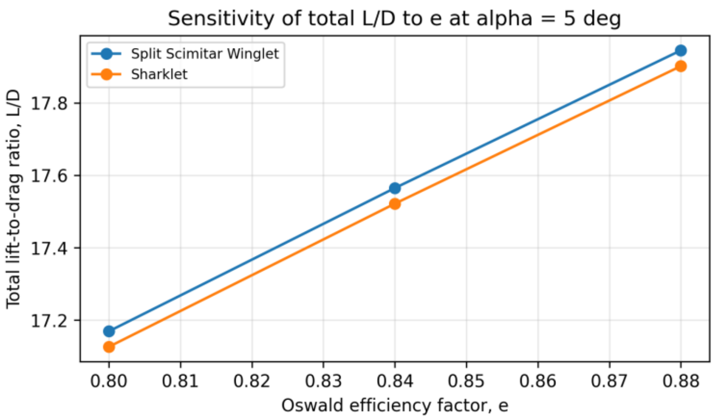

Figure 9. *Sensitivity of total lift-to-drag ratio to Oswald efficiency factor at alpha = 5 deg.*

Figures 10 and 11 show the sensitivity of total C_D and total L/D to effective aspect ratio. Increasing AR from 8.50 to 10.00 decreased total drag and increased total efficiency. This result supports the interpretation that a winglet can be conceptualised as a device that improves effective aspect ratio without requiring the same increase in structural span. The interpretation is consistent with NASA Glenn Research Center's description of winglets as devices that reduce the strength of the tip vortex and with the classical relation showing that induced drag decreases when aspect ratio increases. The result also explains why the split scimitar representation produced slightly higher efficiency under the present input assumptions: its effective aspect ratio and efficiency factor were both slightly higher.

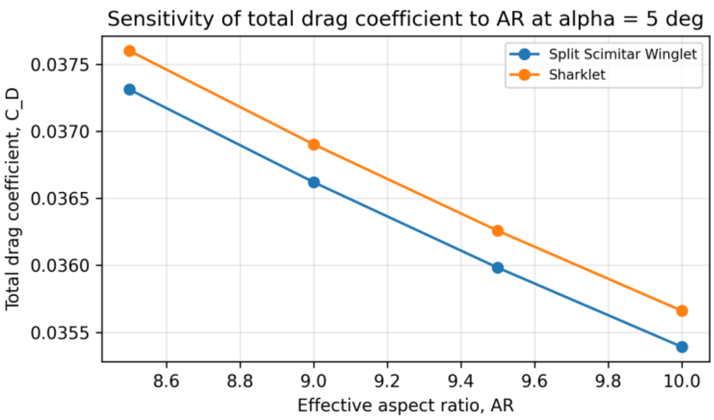

Figure 10. *Sensitivity of total drag coefficient to effective aspect ratio at alpha = 5 deg.*

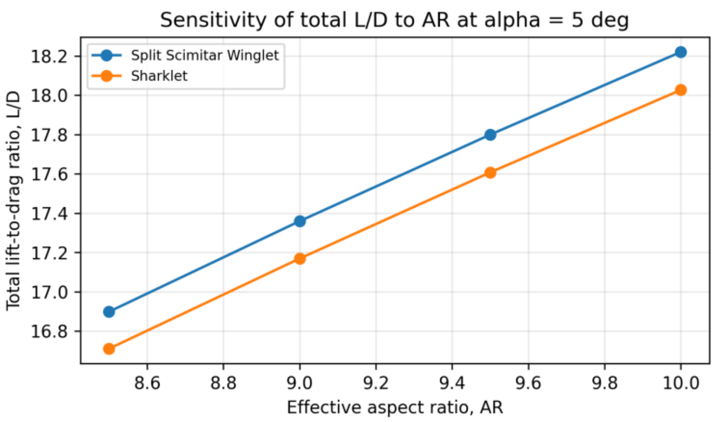

Figure 11. *Sensitivity of total lift-to-drag ratio to effective aspect ratio at alpha = 5 deg.*

Table 6 summarises the sensitivity results. The trend is consistent for both winglet representations, which supports the reliability of the low-order implementation. The model successfully reproduces the expected direction of change: increasing e and AR reduces induced drag and increases aerodynamic efficiency. However, this trend validation is not equivalent to geometry-resolved validation. The model can confirm whether the equations are implemented correctly and whether the resulting trends agree with theory, but it cannot identify local pressure distribution, vortex core structure, shock-related effects, transition, boundary-layer separation, aeroelastic response, or full aircraft performance.

Table 6. Summary of parameter sensitivity at alpha = 5 deg

Parameter Varied	Variation Range	Numerical Trend	Physical Interpretation
Oswald efficiency factor, e	0.80, 0.84, 0.88	C_D decreases and total L/D increases	A more efficient spanwise lift distribution lowers induced losses
Effective aspect ratio, AR	8.50, 9.00, 9.50, 10.00	C_D decreases and total L/D increases	A higher effective aspect ratio reduces the induced-drag component

The comparison with the literature strengthens the interpretation of the results while preserving the correct boundary of the model. Guerrero et al. (2018) and Guerrero et al. (2020) demonstrated through CFD that winglet cant angle and operating condition influence total drag reduction and flight performance. Vaezi et al. (2025) further showed that angle of attack and winglet cant angle are major factors for lift-to-drag response within a broader aerodynamic and aeroacoustic screening framework. The present study does not reproduce their CFD results, but it agrees with their qualitative conclusion that winglet-related parameters and angle of attack must be considered together. The difference is methodological: the present study emphasises transparent low-order calculation and educational reproducibility, whereas those studies emphasise geometry-resolved numerical simulation.

The novelty claim is therefore not that the equations themselves are new. The finite-wing lift relation, induced-drag relation, and aerodynamic force equations are established. The novelty is located in the article-scale integration and operationalisation of those equations into a compact Python workflow for direct comparison between split scimitar and sharklet representations. Table 7 provides a comparative novelty matrix. The matrix shows that the present study contributes a reproducible, low-barrier computational framework that can be used before CFD. This framework is particularly useful in engineering education and early design screening because it reveals cause-and-effect relationships without requiring a complex solver.

Table 7. Comparative evidence for the novelty claim

Aspect	CFD-Based Winglet Studies	Vortex-Lattice or Medium-Order Studies	Present Low-Order Python Study
Geometry detail	High; geometry and mesh are usually required	Moderate; lifting surfaces are discretised	Low; winglets are represented by AR and e
Computational cost	High to moderate	Moderate	Low

Aspect	CFD-Based Winglet Studies	Vortex-Lattice or Medium-Order Studies	Present Low-Order Python Study
Required software	CFD solver and meshing tools	Specialised aerodynamic code or implementation	Standard Python scientific stack
Output focus	Pressure field, drag, lift, vortex, acoustic or detailed flow metrics	Lifting-surface loads and aerodynamic coefficients	C_L, C_Di, C_D, forces, L/D, regression, sensitivity
Educational transparency	Often limited by solver complexity	Moderate	High because every equation is visible
Validation strength	Can include mesh independence and solver comparison	Can include benchmark comparison	Limited to theoretical trend and literature-consistency checks
Contribution of this article	Not intended to replace CFD	Not intended to replace VLM	Provides a reproducible pre-CFD screening workflow for split scimitar versus sharklet representations

The practical implication for engineering computation is that the model can serve as a bridge between theoretical aerodynamics and high-fidelity simulation. Students can observe how changing AR and e affects induced drag and total efficiency. Researchers can use the framework as a preliminary tool to identify whether a parameter set is worth investigating further through CFD. Instructors can use the model to teach finite-wing correction, drag polar reasoning, polynomial approximation, sensitivity analysis, and the difference between internal consistency and external validation. From a design perspective, the method does not provide final certification-grade performance data, but it can reduce conceptual ambiguity before more expensive analysis is conducted.

The limitations of the model must be retained because they define the credibility of the article. Table 8 lists the main limitations and their implications. These limitations prevent overclaiming and help the reader understand the intended function of the model. The most important limitation is the representation of winglet geometry. A split scimitar winglet and a sharklet are geometrically complex devices, but the present model reduces their effect to AR and e. This simplification makes the calculation transparent but removes local geometry effects such as sweep, cant, toe angle, curvature, junction interference, wetted area, and vortex-core trajectory.

Table 8. Model limitations and their effects on interpretation

Aspect	Limitation	Effect on Interpretation
Geometric representation	Winglets are represented through e and AR rather than three-dimensional CAD geometry	Results show numerical trends, not local flow-field details
Flow model	The model does not solve the Navier-Stokes equations	Pressure distribution, turbulence, shock effects, and separation cannot be predicted
Angle-of-attack range	Only 0 deg, 5 deg, and 10 deg are simulated	Polynomial optimum is preliminary and should not be treated as final

Aspect	Limitation	Effect on Interpretation
Drag model	Total drag is simplified as C_D0 + C_Di	Profile drag, interference drag, compressibility drag, and wave drag are not separately resolved
Validation	No CFD mesh independence test or wind-tunnel comparison is performed	Results require external validation before being used for design decisions
Aircraft representation	B737NG and A320 are represented through simplified wing parameters	Results do not claim actual aircraft certification performance

The results should therefore be interpreted as comparative low-order tendencies. Under the input assumptions used, the split scimitar representation produced slightly better total L/D than the sharklet representation. This does not mean that a split scimitar winglet is always superior in actual operation. Actual performance depends on detailed geometry, mission profile, cruise Mach number, Reynolds number, structural integration, aircraft weight, engine-airframe interaction, and operational envelope. The valid conclusion is narrower but defensible: when represented by slightly higher effective aspect ratio and Oswald efficiency factor in this low-order framework, the split scimitar winglet produces a slightly lower total drag coefficient and a slightly higher total lift-to-drag ratio than the sharklet representation.

The reproducibility implication is that every numerical output can be audited from the reported input parameters and governing equations. This property is especially relevant for low-order computational papers because opaque parameter choices can lead to apparently precise results that are not independently verifiable. By retaining the input table, pseudocode, equations, sensitivity analysis, and limitation matrix, the study separates calculable trends from unsupported design claims and provides a tractable base for later CFD or wind-tunnel validation.

An additional implication concerns variable hierarchy. In the present model, the winglet label itself does not directly change the output unless it is translated into physically meaningful parameters such as effective aspect ratio and Oswald efficiency factor. This point is important for engineering interpretation because a named commercial device cannot be evaluated only by its label. The aerodynamic consequence appears through how the device changes span efficiency, induced losses, and the balance between lift growth and drag growth. Therefore, the proposed framework encourages parameter-based reasoning rather than purely descriptive comparison. This reasoning is useful when later studies replace the simplified parameter representation with CAD geometry, CFD mesh refinement, and experimental validation.

IV. CONCLUSION

This study developed and documented a low-order Python numerical framework for comparing split scimitar winglet and sharklet representations through finite-wing aerodynamic parameters. The model calculated lift coefficient, induced drag coefficient, total drag coefficient, lift force, drag force, induced-drag-based efficiency ratio, and total lift-to-drag ratio at angles of attack of 0 deg, 5 deg, and 10 deg. The results showed that lift coefficient increased with angle of attack, while total drag coefficient increased because induced drag depended quadratically on lift coefficient.

The highest total lift-to-drag ratio in the main discrete simulation occurred at 5 deg. The split scimitar winglet representation produced total $L/D = 17.7567$, while the sharklet representation produced total $L/D = 17.5217$. The difference was approximately 1.34% relative to the sharklet value under the same controlled assumptions. A second-order polynomial fitted to the total L/D values estimated local maxima at approximately 6.83 deg for the split scimitar representation and 6.79 deg for the sharklet representation. These values should be treated as preliminary screening estimates rather than final optimum angles.

Sensitivity analysis confirmed that increasing the Oswald efficiency factor and effective aspect ratio reduced total drag and increased total lift-to-drag ratio. This behaviour agrees with finite-wing theory and supports the internal consistency of the Python implementation. The main contribution of the study is methodological and educational: it provides a transparent, reproducible, and low-barrier framework for linking finite-wing equations, polynomial estimation, and sensitivity analysis in one article-scale workflow. Future research should extend the angle-of-attack grid, include geometry-resolved CAD models, conduct CFD simulations with mesh independence testing, compare the outputs with wind-tunnel or validated numerical data, and examine additional operational variables such as Mach number, Reynolds number, payload condition, and mission segment.

V. ACKNOWLEDGEMENTS

The authors thank the academic environment of the Mechanical Engineering Master's Programme at Universitas Negeri Malang for supporting discussions on numerical methods, engineering simulation, regression analysis, and aerodynamic interpretation. No additional non-author contribution altered the scientific content of this manuscript.

VI. REFERENCES

[1] Abbott, I. H., & von Doenhoff, A. E. (1959). *Theory of wing sections: Including a summary of airfoil data*. Dover Publications.

[2] Anderson, J. D. (2017). *Fundamentals of aerodynamics* (6th ed.). McGraw-Hill Education.

[3] Gao, W., Liu, Y., Li, Q., & Lu, B. (2023). Aerodynamic modeling and simulation of multi-lifting surfaces based on the unsteady vortex lattice method. *Aerospace, 10*(2), 203. https://doi.org/10.3390/aerospace10020203

[4] Guerrero, J. E., Sanguineti, M., & Wittkowski, K. (2018). CFD study of the impact of variable cant angle winglets on total drag reduction. *Aerospace, 5*(4), 126. https://doi.org/10.3390/aerospace5040126

[5] Guerrero, J. E., Sanguineti, M., & Wittkowski, K. (2020). Variable cant angle winglets for improvement of aircraft flight performance. *Meccanica, 55*(10), 1917-1947. https://doi.org/10.1007/s11012-020-01230-1

[6] Hoerner, S. F. (1965). *Fluid-dynamic drag: Practical information on aerodynamic drag and hydrodynamic resistance*. Hoerner Fluid Dynamics.

[7] Joshi, H., & Thomas, P. (2023). Review of vortex lattice method for supersonic aircraft design. *The Aeronautical Journal, 127*(1317), 1869-1903. https://doi.org/10.1017/aer.2023.25

[8] NASA Glenn Research Center. (2023a, January 21). *Modern drag equation*. https://www1.grc.nasa.gov/beginners-guide-to-aeronautics/modern-drag-equation/

[9] NASA Glenn Research Center. (2023b, July 27). *Induced drag coefficient*. https://www1.grc.nasa.gov/beginners-guide-to-aeronautics/induced-drag-coefficient/

[10] NASA Glenn Research Center. (2024, July 19). *Lift to drag ratio*. https://www1.grc.nasa.gov/beginners-guide-to-aeronautics/lift-to-drag-ratio/

[11] NASA Glenn Research Center. (2025a, July 1). *Drag equation*. https://www1.grc.nasa.gov/beginners-guide-to-aeronautics/drag-equation/

[12] NASA Glenn Research Center. (2025b, July 7). *Winglets*. https://www1.grc.nasa.gov/beginners-guide-to-aeronautics/winglets/

[13] Vaezi, E., Madani, S. A. S., & Keshmiri, A. (2025). A parametric study on the effects of winglet cant angle on wing aerodynamics and aeroacoustics. *Scientific Reports, 15*, 1417. https://doi.org/10.1038/s41598-024-84453-6

[14] Whitcomb, R. T. (1976). *A design approach and selected wind-tunnel results at high subsonic speeds for wing-tip mounted winglets* (NASA Technical Note D-8260). National Aeronautics and Space Administration.